Applied Catalysis B: Environmental 100 (2010) 47–54

Contents lists available at ScienceDirect

Applied Catalysis B: Environmental

journal homepage: www.elsevier.com/locate/apcatb

Assessing optimal photoactivity on titania nanotubes using different annealing temperatures

J.A. Toledo Antonio [a,*], M.A. Cortes-Jacome [a], S.L. Orozco-Cerros [b], E. Montiel-Palacios [b], R. Suarez-Parra [b], C. Angeles-Chavez [a], J. Navarete [a], E. López-Salinas [a]

[a] Molecular Engineering Program, Instituto Mexicano del Petróleo, Eje Central Lázaro Cárdenas # 152, San Bartolo Atepehuacan, G.A. Madero, 07730 México, D.F., Mexico
[b] Centro de Investigación en Energía, Universidad Nacional Autónoma de México, Apartado Postal 34, Temixco 62580, Morelos, Mexico

ARTICLE INFO

Article history:
Received 12 May 2009
Received in revised form 28 June 2010
Accepted 13 July 2010
Available online 21 July 2010

Keywords:
Photocatalysis
Titania nanotubes
Azo dye degradation
UV–vis

ABSTRACT

Photocatalytic activity of titania nanotubes, during degradation of reactive blue 69 (RB-69) dyes, was correlated with its optical properties and compared with commercial photocatalyst P25. Titania nanotubes made up of two structural layers walls were prepared by an alkali thermal reflux treatment at atmospheric pressure from an anatase precursor with sodium hydroxide. Annealing titania nanotubes at 473–673 K, red-shifted the fundamental transition edge of titania, showing a maximum at 573 K with a band gap energy of 2.97 eV and an additional visible absorption band was originated due to the dehydroxylation of strongly deformed TiO_6 octahedral layers on the curved nanotubular structure. Temperatures above 673 K brought about the collapse of TiO_6 octahedra layers of the nanotubular walls yielding anatase domains inhibiting the light absorption in the visible region and blue shifting the UV absorption to a band gap energy of 3.2 eV. The higher the red-shift of the transition edge of titania the higher the photocatalytic activity in degradation of the dye compound. Titania nanotubes annealed at 573 K showed similar photodegradation activity (per mass unit) of RB-69 to commercial photocatalysts Degussa-P25, both with band gap energies of 2.97 and 3.0 eV, respectively.

1. Introduction

Titanium oxides have attracted considerable attention because of their multiple potential applications. They have been used as semiconductor materials in the construction of electronics devices [1], in the manufacturing of pigments and coatings [2], in solar cells [3], sensors [4], cosmetics, as catalysts support in several processes [5–8], and particularly as photocatalysts in the degradation of organic compounds in environmental protection processes [9]. The catalytic functions of the aforementioned systems can be upgraded when the titanium oxides' structure shift towards nanoscale range [10]. In fact, downsizing material structures of the same chemical elements modify their mechanical, optical, magnetic and electronic properties as well as their chemical reactivity, which in turn lead to surprising and unpredictable effects [11]. Additionally and in the case of the same chemical elements, the conversion of tridimensionally (3D) structured inorganic materials into one dimensional (1D) structures, such as nanotubes [12] change significantly their optical properties because strongly deformed structure at the curvature of nanotubular walls and confinement effects, and the increase in specific surface area [12].

Inspired on the mimic of natural photosynthesis processes, a great interest has been focused on searching semiconducting materials capable to catalyze efficient visible light photoredox reaction. Among the various metal oxide photocatalysts, titanium oxide is a semiconductor material widely used to fully oxidize waste organic compounds in water [13], and it still remains as the most promising photocatalyst owing to its low cost, chemical inertness, null toxicity and high photostability [13–16]. TiO_2, as anatase phase, presents an absorption band edge at 387 nm, corresponding to band gap energy of 3.2 eV, and as rutile phase, its absorption edge red-shift slightly showing band gap energy at 3.0 eV. Therefore, either rutile or anatase requires ultraviolet (UV) light irradiation to generate electron–hole pairs and to promote photocatalytic activity. Moreover, in the solar energy spectrum, the UV light accounts for only ca. 4% whereas the visible light accounts ca. 45%. Therefore, any shift in optical response from UV to visible region is expected to impact positively on the photocatalytic efficiencies of the TiO_2 based semiconductors [17]. Then, for a more efficient utilization of the visible light in photocatalytic processes, it is necessary to look for a modified titania exhibiting a strong red-shift and strong band-to-band absorption [18].

Several approaches have been attempted on the bulk and surface modification of titania by doping with different elements like carbon [19–21], sulfur [22–24] and nitrogen [17,24–28], by adding transition metal oxides such as Fe_2O_3, ZnO, Cr_2O_3, WO_3, CuO, SiO_2,

* Corresponding author. Tel.: +52 55 91 75 84 34.
E-mail address: jtoledo@imp.mx (J.A. Toledo Antonio).

0926-3373/$ – see front matter © 2010 Elsevier B.V. All rights reserved.
doi:10.1016/j.apcatb.2010.07.009

etc. [29–35], or by adding gold or silver nanoparticles [36–41]. These strategies generate localized electronic states "surface states" close to the valence band edge, red-shifting the absorption band edge of titania and inducing the appearance of a broad absorption band in the visible region at the low energy side (>400 nm). When the band gap energy of titania red-shift from 3.2 to 2.2 eV for anatase and nitrogen-doped anatase, respectively, the ability of the later to degrade organic compounds in waste water and air pollutants increase considerably [27].

The transformation of anatase into nanotubes by a simple alkaline hydrothermal method [42,43] yielded materials with specific surface area as large as 425 m^2/g [44,45] exhibiting large internal and external surfaces, along with surface in the vertex and surface in the interlayer regions that made up the nanotube walls. These nanotubular features of TiO_2 provide both a large amount of adsorbates and channels for enhanced electron transfer, which play an important role during oxidation of organic compounds in photocatalytic reactions. Additionally, titania nanotubes' structure contains large amounts of OH groups on the interlayer region of the walls which are likely to inhibit the recombination rate of the photogenerated electrons (e^-) and holes (h^+) pairs. Also, the free movement of the charge carriers throughout the length of the nanotubes, is expected to reduce the charge recombination probability [46].

Several research groups have pointed out the enhanced photocatalytic activity of titania nanotubes compared with that of anatase nanoparticles [46–51] during the degradation processes of an organic compound under UV light. These results have been rationalized in terms of charge recombination dynamics between the radical cation and e^-, which were observed living longer in nanotubes than in nanoparticles [46]. Recently, it has been reported that the Ti–OH bonds in the nanotubes act as photoluminescent sites [47]. From these studies it can be established that titania nanotubes are able to absorb and emit light in the visible region, suggesting that its intrinsic photocatalytic activity (e.g. without addition of foreign anions, cations or metals nanoparticles) can be activated under sun light, and that the morphology of nanotubes and the remaining OH groups inhibit the charge recombination rate.

In this work, titania nanotubes were annealed at different temperatures with a view to generate an optimal photocatalytic activity. The photocatalytic activity of nanotubes annealed at different temperatures was measured in the degradation of reactive blue 69 dye under UV light (370 nm). The photocatalytic activity was compared with that of a commercial photocatalyst TiO_2 Degussa-P25. The results were discussed in terms of the remaining OH groups and Na^+ ions in the interlayer space of nanotubes, acting as nanotubular structure stabilizer of strongly deformed TiO_6 octahedra layers of the curved structure and also as inhibitor of the charge recombination during the photocatalytic process.

2. Experimental

2.1. Synthesis of titania nanotubes

Nanotubular titania was synthesized by thermal refluxing an anatase precursor with crystallite size of 22.0 nm (as determined by XRD Rietveld Refinement analysis) with a NaOH solution under atmospheric pressure. Forty-five grams of TiO_2 anatase powder was suspended in 3 L of an aqueous 10 M NaOH solution and the resulting suspension was placed in 4 L glass vessel under reflux. The refluxing reaction was conducted at 373 K, during 18 h under stirring at 200 rpm. Then, the white slurry was filtered and neutralized with a 1 M solution of hydrochloric acid until the pH was lowered to 3.0. The resulting suspension was maintained at this pH overnight under continuous stirring. The material was repeatedly washed with abundant deionized water until it was chlorine-free, i.e. by testing with silver nitrate solution. The material was finally dried at 373 K overnight, yielding a hydrous titania powder with nanotubular morphology.

2.2. Raman spectroscopy

The Raman spectra were recorded using an Yvon Jobin Horiba (T64000) spectrometer, equipped with a confocal microscope (Olympus, BX41) with an Ar ion laser operating at 514.5 nm at a power level of 10 mW. The spectrometer is equipped with a CCD camera detector. Powdered titania nanotubes were placed in a Linkam cell stage directly adapted to the microscope of the instrument, which provides controlled atmosphere and temperature. The glass window of the cell was 1 mm thick.

2.3. High resolution transmission electron microscopy

High resolution transmission electron microscopy (HRTEM) analysis was performed in a JEM2200FS transmission electron microscope operating at 200 kV, and equipped with a Schottky-type field emission gun and an ultrahigh resolution pole piece (Cs = 0.5 mm; point-to-point resolution, 0.190 nm). The samples were ground, suspended in isopropanol at room temperature, and dispersed with ultrasonic stirring; then, an aliquot of the solution was dropped on a 3 mm diameter lacey carbon copper grid. Chemical analysis by energy dispersive X-ray spectroscopy (EDXS) was performed in an environmental scanning electro microscope XL30.

2.4. UV–vis–DRS measurements

A Perkin Elmer, lambda 900, UV–vis spectrometer was used to directly record the diffuse reflectance spectra (DRS). Samples were in situ annealed in a home made cell equipped with a quartz window, by flowing nitrogen during the thermal treatment at temperatures ranging from 373 to 773 K, in order to eliminate the contribution of OH groups from environmental water absorption, given the highly hydrophilic nature of titania nanotubes.

2.5. Photodegradation test

The photocatalytic activity of TiO_2 nanotubes, as prepared and annealed at indicated temperatures, was evaluated by the degradation of a dye, reactive blue 69 (RB-69) dye, also known as blue-lanasol, and compared with that of a commercial TiO_2 Degussa-P25. The reaction proceeded at pH = 2.8, over 0.4 g/L of catalyst, 100 mg/L of RB-69 and 320 mg/L of hydrogen peroxide as an oxidant agent. The pH was attained with diluted sulfuric acid and then the suspension was exposed to UV light from a 15W domestic lamp (Sanelec). To characterize the emission spectrum of the lamp a Shimadzu mod. UV-3101 PC UV–vis–IR spectrophotometer was used. Maximal photonic flux of 3.5×10^{-5} E s^{-1} μm^{-1} was used to estimate the photocatalytic activity of TiO_2 nanotubes.

To determine the RB-69 concentration during the photocatalytic process, a sample, from the reactor was centrifuged to remove the catalyst and the remnant was immediately analyzed using its characteristic absorption peak at λ_{car} = 605 nm. The absorption spectra were measured in the wavelength range 200–700 nm with a Hach DR 5000 Spectrophotometer, using a spectral interval of 2 nm. The mineralization degree of RB-69 was determined by measurements of the total organic carbon (TOC) with Hatch direct method, for low (0.3–20 mg/L) and mid (15–150 mg/L) range. In parallel, chemical

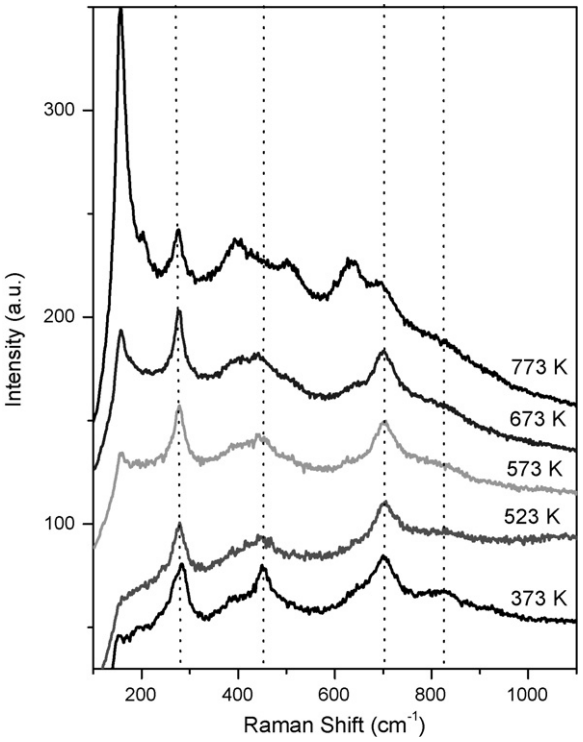

Fig. 1. Raman spectra of titania nanotubes annealed at indicated temperatures.

oxygen demand (COD) was determined in accordance with standard test methods [52].

3. Results and discussion

3.1. Structure

Raman spectroscopy is the most suitable technique to study the structure layered titanates and their derivatives titania nanotubes [53,54], due to the microcrystalline nature of the nanotubes and their Raman characteristic bands, which totally differ from those of anatase, in contrast in X-ray diffraction the more intense peaks around $2\theta = 24–25.5^\circ$ and 48.5° overlap with the (1 0 1) and (2 0 0) diffraction lines of anatase and frequently the structure of titania nanotubes are confused with that of anatase [42,55,56]. The most representative Raman bands of titania nanoubes occurs at 278, 450 and 704 cm^{-1} (see dotted straight lines in Fig. 1), which totally differs from the Raman active modes of anatase precursor, which occur at 144, 200, 400, 505, 640 and 796 cm^{-1}. The Raman band at 704 cm^{-1} in the nanotubular structure has been assigned to totally symmetric Ti–O vibration from the A_g symmetric modes of the TiO_6 octahedra on the layered structure [53], whereas those at 450 an 278 cm^{-1} have been assigned to the splitting of the degenerate mode of TiO_6 octahedra in the layered structure of titania nanotubes. After in situ annealing at 523 K, the spectrum remain unchanged, only the band at 450 cm^{-1} broadened with intensity decrease. After annealing at 573 K, the nanotubular structure started to reconvert into anatase, which was evident by the appearing of a Raman band at 156 cm^{-1}, characteristic of the A_{1g} active mode of Ti–O–Ti in anatase structure (see Fig. 1). The intensity of this Raman band increased after annealing at 673 K suggesting a higher degree of transformation of the layered titanate into anatase micro-domains in regions where the layered structures collapsed, and that both anatase and layered titanate phases coexist in the samples after annealing at 673 K.

3.2. Morphology

Nanotubular features of the as synthesized sample are shown in Fig. 2a. All the nanotubes are composed by only two structural layers with an interlayer distance of 0.76 nm (see inset in Fig. 2a). The inner diameter of the nanotubes is around 5.0 nm whereas the outer diameter is around 8.0 nm. The thickness of the nanotubular walls is around 1.5 nm composed by two layers of TiO_6 octahedra. After annealing at 573 K (see Fig. 2b) the space between the two TiO_6 octahedra layers disappeared, yielding anatase domains in the nanotubular walls, which are most evident in the nanotubes of the sample annealed at 673 K, where still the main nanotubular features of the sample were maintained (see Fig. 2c).

3.3. Optical properties

UV–vis spectra of in situ nitrogen annealed samples at different temperatures are presented in Fig. 3. The as synthesized nanotubes annealed at 373 K showed a low intensity absorption band, blue-shifted in comparison with that shown by reference anatase phase. Additional to the fundamental absorption edge of the titania, a new absorption band was observed in the visible range of 400–700 nm after in situ annealing nanotubes at 473, 573 and 673 K showing a maximum in absorption intensity at 573 K. At higher temperatures, the intensity of the visible absorption band decreased at 673 K and it completely disappeared after annealing at 773 K, showing absorption only in the UV region, with a fundamental edge transition characteristic of anatase phase at 387 nm. These results can be rationalized as follows: in the as synthesized nanotubes, large amount of physisorbed water remain in the inner and outer surfaces of titania nanotubes, quenching the UV absorption and also blue shifting the titania absorption edge in comparison to that of anatase phase. At higher annealing temperatures, physisorbed water is removed and consequently the OH group density in the nanotubular structure drops [47]. Therefore, the nanotubular titania edge transition red-shifts and an absorption band in the visible region appears reaching a maximum after annealing at 573 K. As indicated in our Raman results in Fig. 1, the maximum temperature at which nanotubular structure remains stable, without extensive retransformation into anatase, is 573 K. After annealing at 673 and 773 K, the intensity of the absorption in the visible region considerably dropped because the nanotubular structure collapsed into anatase (see Fig. 1). Notwithstanding, the nanotubular morphology was maintained as observed in the TEM images in Fig. 2b. In fact, after annealing at 773 K, where Raman spectra indicated anatase as the major phase, titania nanotubes showed exactly the same absorption edge as the anatase used as reference.

Kubelka–Munk function versus the band gap energy is shown in inset of Fig. 3. The extrapolation of the modified spectra to zero absorption determines the band gap energy (BGE) of the fundamental transition edges of nanotubes as function of the annealing temperature. The as synthesized nanotubes dried at 373 K showed a BGE of 3.5 eV, larger than that of anatase phase (3.2 eV). When heat-treating the nanotubes at higher temperatures however, the BGE decreased and reached a minimum value of 2.9 eV (i.e. at 573 K). Thereafter, BGE was 3.2 eV at 773 K, i.e. the characteristic BGE of anatase phase. The maximum red-shift absorption was obtained after annealing nanotubes at 573 K, with a BGE of 2.9 eV, quite similar to the energy value of commercially available photocatalyst TiO_2 Degussa-P25 (i.e. 3.0 eV).

The dehydroxylation of nanotubular structure during annealing treatment at temperatures 473–673 K, brings about the breaking Ti–OH bonds, yielding Ti–O–Ti bonds. Concomitantly, oxygen vacancy sites are generated in the strongly deformed TiO_6 octahe-

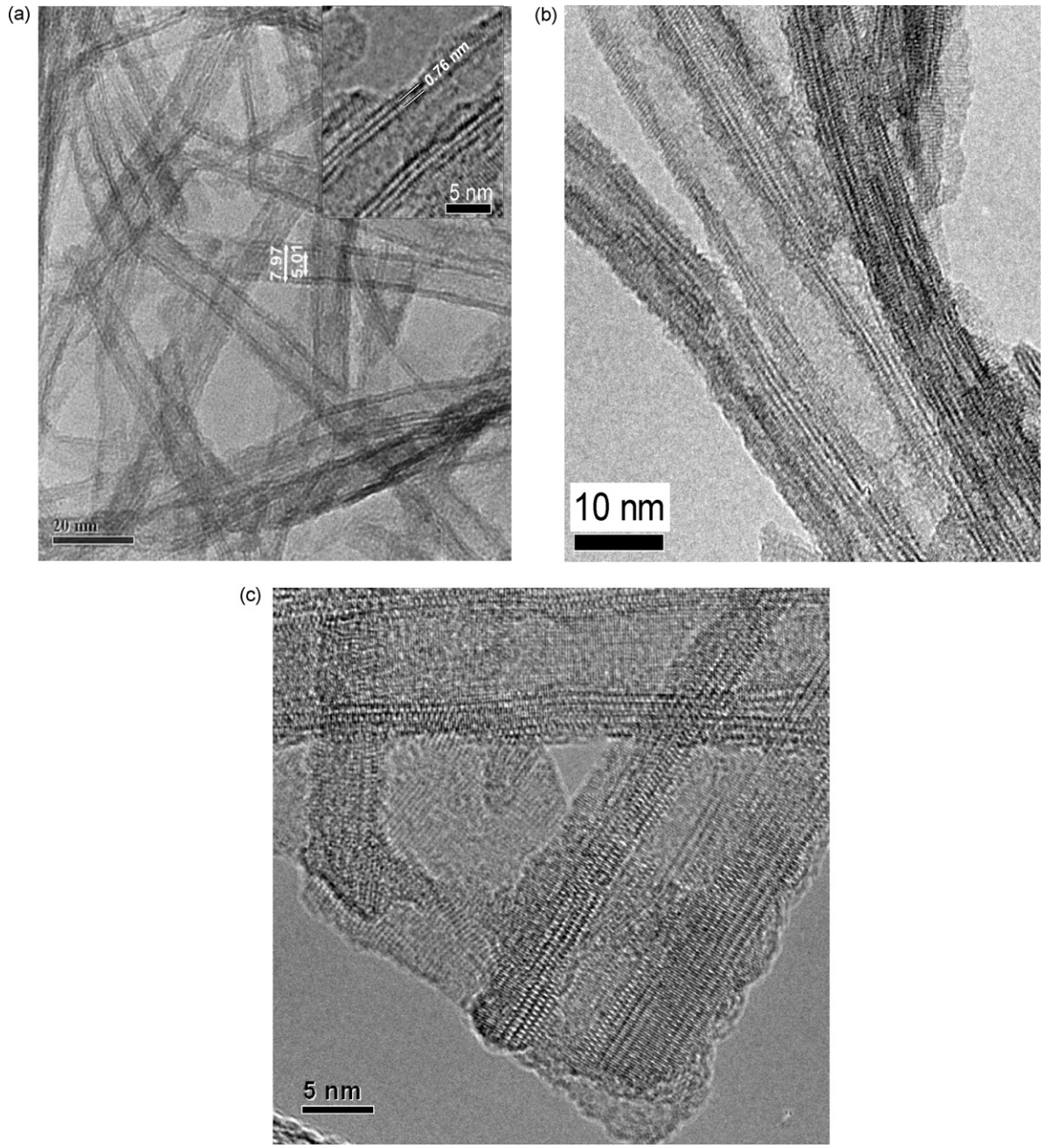

Fig. 2. TEM images of: (a) As made titania nanotubes dried at 373 K (inset is an amplification of isolated nanotubes), (b) after annealing at 573 K and (c) after annealing at 673 K.

dral layers of the curved nanotubular walls. Seemingly, the red-shift of UV absorption and the appearance of visible region absorption are related to the nanotubular structure with strongly deformed TiO_6 octahedral layers its walls, which in turns depend on the degree of dehydroxylation. Dehydroxylation at high temperature induces the collapse of the nanotubular array; formal bonds are produced between each layer of TiO_6 octahedral yielding anatase domains on the nanotubular walls. The TiO_6 octahedral deformation decreases in the anatase domains reducing the amount of oxygen vacancy sites, then, the UV absorption blue shifts to the value characteristic of anatase phase (e.g. 387 nm), and the absorption in the visible region decreases gradually and it completely disappears after annealing at 773 K, where the material are almost completely transformed into anatase, as indicated by our Raman results in Fig. 1.

3.4. Photocatalytic activity

Since the annealing process is a critical condition that modifies the UV and visible light absorption of the TiO_2 nanotubes, it is also important to consider the photocatalytic properties of TiO_2 nanotubes before the heat-treatment step. In order to assess the photocatalytic activity of as prepared and annealed TiO_2 nanotubes, first the optimal concentration of catalyst was determined, using Degussa-P25 as a reference. The obtained results suggested that using 0.4 g/L of catalyst Degussa-P25 is enough to eliminate, in 2.5 h, 100 mg/L of the RB-69. Higher concentrations of catalyst Degussa-P25 (0.6 g/L) did not improve the photodegradation time of RB-69.

The decolorization curves of RB-69 using fresh and annealed TiO_2 nanotubes were compared with TiO_2 Degussa-P25. The evo-

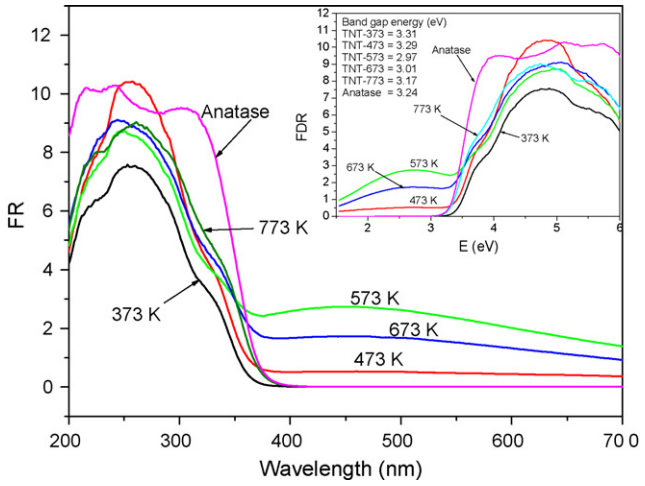

Fig. 3. UV–vis–DR spectra of titania nanotubes in situ annealed at indicated temperatures. Inset shows plots of transformed Kubelka–Munk function versus photon energy.

lution of the dye decolorization was followed measuring the maximum absorbance peak in the visible region at $\lambda = 605$ nm. At this wavelength, the chromophore group of the RB-69 molecule absorbs and its concentration is proportional to the measured absorbance. Fig. 4 illustrates the UV–vis absorbance spectrum during the RB-69 decolorization using: (a) nanotubes of TiO_2 annealed at 573 K and (b) TiO_2 Degussa-P25. In this figure the decrease of the absorbance peak at $\lambda = 605$ nm can be observed. The catalyst, TiO_2 Degussa-P25 not only shows the breakdown of the chromophore group but also the intermediate compounds, as a major shift of bands can be noted in the UV absorbance spectrum region (see Fig. 4). Fig. 5 depicts the decolorization profiles of RB-69 as a function of time with TiO_2 nanotubes dried at 373 K (TNT 373 K) and annealed at 473 K (TNT 473 K), 573 K (TNT 573 K), and TiO_2 Degussa-P25. As can be noticed in Fig. 5, the photocatalytic activity of TiO_2 nanotubes improves along the annealing temperature. TiO_2 nanotubes annealed at 473 K showed better photocatalytic activity in the first half of the photodegradation process than TiO_2 nanotubes dried at 373 K, however, 2.5 h of reaction, both catalysts eliminated similar quantities of the dye. On the other hand, the photocatalytic activity of TiO_2 nanotubes significantly increased when they were annealed at 573 K. The commercial TiO_2 Degussa-P25 and TiO_2 nanotubes annealed at 573 K show a similar photocatalytic activity to eliminate the RB-69 compound. This result is visibly noticed as the mixtures are colorless after 2.5 h of the photodegradation processes. In addition, the TiO_2 nanotubes were also annealed at 673 and 773 K, but their photocatalytic activity showed a substantial drop; they only eliminate 35% of RB-69, in the same period of time, as can be observed in Fig. 5 for TNT 673 K.

In order to eliminate the influence of the emitted radiation in the photodegradation of RB-69, the emission spectrum of the domestic lamp used in this study was measured and reported in Fig. 6. The decomposition of the RB-69 by photolysis in hydrogen peroxide, without any catalyst, did not proceed with the selected lamp, as it does not emit the necessary UV radiation to carry out the RB-69 photodegradation, in water solution, in the same interval of time (see Fig. 5).

In order to determine the quality of the treated water, complementary analysis of chemical oxygen demand (COD) was made. Total organic carbon (TOC) was also determined at the beginning and after 300 min of the photodegradation process.

The evolution of COD on the as prepared and annealed TiO_2 nanotubes and TiO_2 Degussa -P25 is shown in Fig. 7. These results demonstrate that for the first 120 min all TiO_2 nanotubes give a

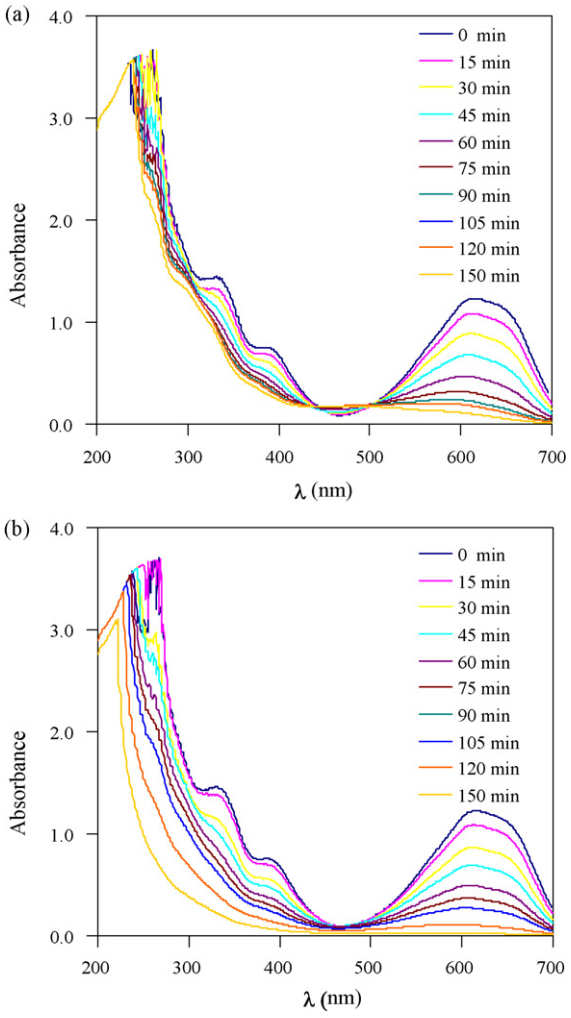

Fig. 4. UV–vis absorbance spectra during the decolorization of RB-69 using: (a) TiO_2 nanotubes annealed at 573 K and (b) TiO_2 Degussa-P25.

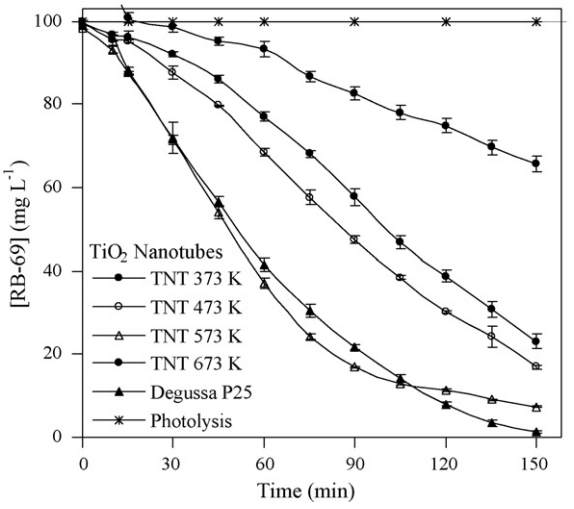

Fig. 5. Decolorization profiles of RB-69 with titania nanotubes annealed at different temperatures as a function of time.

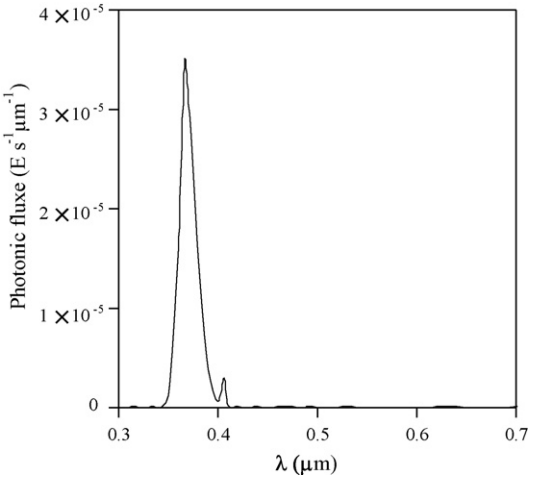

Fig. 6. Emission spectrum of the UV lamp.

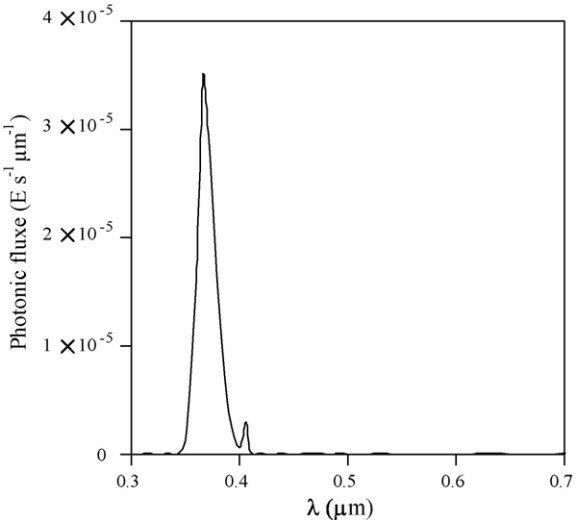

Fig. 7. Chemical oxygen demand as a function of the photodegradation time of RB-69 on TiO_2 nanotubes annealed at indicated temperatures.

lower COD than TiO_2 Degussa-P25. Later, the COD profile dropped faster in the photocatalytic degradation for the TiO_2 Degussa-P25 than that using annealed TiO_2 nanotubes. The difference between these results suggests that RB-69 photodegradation was more complete (i.e. with less intermediate degradation products formed) when the catalytic process was carried out on TiO_2 Degussa-P25. Moreover, the TiO_2 nanotubes annealed at 573 K showed the lowest value of COD after 300 min of photocatalytic degradation compared with that on TiO_2 nanotubes annealed at other temperatures.

The RB-69 mineralization degree was determined by measurements of the total organic carbon (TOC) using the Hatch direct method (see Table 1). TOC value was lower when the photocatalytic process was carried out on TiO_2 nanotubes annealed at 573 K than those annealed at other temperatures. However, the lowest TOC values were obtained when using TiO_2 Degussa-P25. This result suggests a better RB-69 degradation into CO_2, H_2O and mineral ions.

Table 1
Total organic carbon (TOC) at the beginning and at the end of the RB-69 photodegradation on titania nanotubes annealed at indicated temperatures.

Catalyst	Initial TOC (mg/L)	Final TOC (mg/L)
TNT-373 K	25	22
TNT-473 K	25	19
TNT-573 K	25	10
TNT-673 K	25	21
TNT-773 K	25	25
TiO_2 Degussa-P25	25	6.5

Table 2
Reaction rate constant k and regression coefficients of RB-69 decolorization with different catalysts.

Catalyst	Rate constant (k) (min^{-1})	Regression coefficient (R^2)
TNT-373 K	0.00776 ± 0.0002	0. 89 ± 0.01
TNT-473 K	0.00978 ± 0.0001	0.92 ± 0.01
TNT-573 K	0.01785 ± 0.0001	0.98 ± 0.01
TNT-673 K	0.00354 ± 0.0001	0.98 ± 0.001
TNT-773 K	0.00253 ± 0.0008	0.93 ± 0.01
TiO_2 Degussa-P25	0.02240 ± 0.0004	0.89 ± 0.02

4. Kinetic studies

The obtained results from the RB-69 decolorization follow a pseudo first order kinetics as a function of concentration for all the TiO_2 catalysts:

$$-\frac{d[\text{RB-69}]}{dt} = k[\text{RB-69}] \quad (1)$$

$$\text{Ln}\frac{[\text{RB-69}]_0}{[\text{RB-69}]} = kt \quad (2)$$

where k (min^{-1}) is the rate constant.

Eq. (2) gives an exponential decay of the RB-69 as a function of the time. The values of the rate constant, k, and regression coefficient are listed in Table 2. TiO_2 nanotubes annealed at 573 K showed a higher photocatalytic activity than TiO_2 nanotubes heat-treated at 473, 673 and 773 K. However, for the TiO_2 Degussa-P25 and TiO_2 nanotubes annealed at 573 K, the rate constant value is of the same order.

The photocatalytic activity of titania nanotubes strongly depended on the optical properties of UV–vis absorption. In fact, the higher photocatalytic activity in RB-69 degradation is likely due to the higher red-shift of the fundamental absorption transition of titania nanotubes. Then, as the BGE decreased, from 3.5 to 2.9 eV in nanotubes annealed at 373 and 573 K, respectively, the photocatalytic decolorization rate of RB-69 increased gradually. This means that by decreasing the BGE, it is possible to increase the ability of TiO_2 nanotubes to photogenerate electron–hole pairs on the surface, by the action of UV, thus improving the photocatalytic degradation of organic compounds. In fact, for commercial P25, with anatase-rutile phases combination, a BGE of 3.0 eV has been reported, and its photocatalytic activity in decolorization of RB-69 resulted quite similar to that of TNT 573 K (see Fig. 5 and Table 2). Nonetheless, at the end of the reaction, the COD and TOC values for P25 photocatalyst are lower than those for TNT 573 K as can be observed in Fig. 7 and Table 1. At higher annealing temperatures (i.e. at 673 and 773 K), the titania fundamental edge transition blue-shifted to the edge transition of pure anatase, with the consequent drop on the photocatalytic active sites, due to the collapse of the TiO_6 octahedral layers of the nanotube walls yielding anatase domains. Photocatalytic activity and BGE are plotted in Fig. 8 as a function of the annealing temperature, and as can be noted in this figure, the RB-69 degradation rate presents an inverse behavior, compared to the BGE value. Indeed, high annealing temperatures (e.g. 673–773 K) correspond low BGE values in comparison with those obtained at low temperature (373–473 K), at the same time, the photocatalytic activity was higher in samples annealed at 373 and 473 K with high BGE. This behavior can be rationalized as follows: annealing at low temperature preserved the layered nanotubular structure, whereas at high temperature

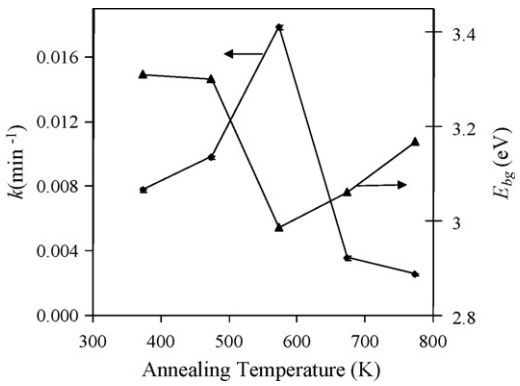

Fig. 8. Reaction rate constant (k) and band gap energy (BGE) as function of TiO_2 nanotubes annealing temperature.

the nanotubular structure partially collapsed into anatase nanoparticles (see Raman results) showing low BGE, however the specific surface area decreased and consequently their photocatalytic activity.

In agreement with our results, low or null photocatalytic activity in aqueous degradation of organic compounds has been reported for as synthesized titania nanotubes or nanowires by alkali hydrothermal method [48,49]. The excess of physisorbed water in the nanotubular interlayer space blocks the UV and visible light absorption, which is characteristic of the deformed TiO_6 octahedron in the strongly curved nanotubular structure. Then, by using an appropriate annealing procedure, structural dehydroxylation can be manipulated to an optimum value to activate the photocatalytic active sites. Accordingly, in anatase, photocatalytic active sites for phenol degradation are improved after annealing at 623–723 K [50] even under visible light illumination, whereas for H-titanate nanowires the optimum photocatalytic activity was obtained after annealing at 773 K [49]. From our results, photocatalytic activity of titania nanotubes is improved after annealing at 573 K, by the optimal dehydroxylation degree of the structural layers, taking care of maintaining the nanotubular structure. The remaining OH groups along with the strongly deformed TiO_6 octahedron in the curved structure of nanotubes acts as light absorption centers, red-shifting the UV–vis absorption and generating light absorption in the visible region, then, the catalytic sites can be photoactivated more efficiently.

In fact, highly crystalline alkali titanates nanowires have shown strong absorption in the visible light region, and consequently high photocatalytic activity under visible light irradiation [51]. As our titania nanotubes were obtained by alkaline hydrothermal method, the residual amount of Na ions, after ion-exchange with HCl, was lower than 1.5 wt.%, as determined by EDXS analysis. Then, the formation of any sodium titanate is unlikely and if it happens, it may be constant in all the samples. Therefore, it is not possible to attribute the high photocatalytic activity to the presence of residual Na^+ ions. Rather Na^+ ions in the interlayer space contribute to stabilize the nanotubular structure maintaining the strongly deformed TiO_6 octahedron on its walls. After annealing at 673 and 773 K, active photocatalytic sites decreased due to the collapse the TiO_6 octahedron layers of the nanotubes walls, yielding 3D anatase domains in which the layer curvature disappeared.

5. Conclusions

The photocatalytic activity of TiO_2 nanotubes can be tuned up by means of manipulating the annealing temperature. When TiO_2 nanotubes are used as catalysts without any annealing treatment, their photocatalytic performance is low in comparison to that of a commercial photocatalyst TiO_2 Degussa-P25 that consists of 75% anatase and 25% rutile. Nevertheless, when TiO_2 nanotubes are annealed at 573 K, the photocatalytic activity becomes very close to that of TiO_2 Degussa-P25. These results are explained in terms of controlling the degree of dehydroxylation of the nanotubes. Moreover, a considerable visible absorption can be generated in TiO_2 nanotubes simply by annealing at 573 K, which does not occur on anatase. At temperatures above 573 K, the visible absorption band almost extinguishes.

Acknowledgments

This work was partially sponsored by IMP's D.00446 and D.00483 projects, and IN114609-3 project from DGAPA-UNAM ,as well as CONACyT Mexico-82909. R. Morán-Elvira 's technical assistance is greatly appreciated. S.L. Orozco-Cerros acknowledges the postdoctoral scholarship program of UNAM.

References

[1] N. Sakai, Y. Ebina, K. Takada, T. Sasaki, J. Am. Chem. Soc. 126 (2004) 5851–5858.
[2] C. Drew, X. Liu, D. Ziegler, X. Wang, F.F. Bruno, J. Whitten, L.A. Samuelson, J. Kumar, Nano Lett. 3 (2003) 143–147.
[3] S. Ushiroda, N. Ruzycki, Y. Lu, M.T. Spitler, B.A. Parkinson, J. Am. Chem. Soc. 127 (2005) 5158–5168.
[4] L. Feng, Y. Liu, J. Hu, Langmuir 20 (2004) 1786–1790.
[5] S. Dzwigaj, C. Luis, M. Breysse, M. Cattenet, V. Belleire, C. Geantet, M. Vrinat, P. Blanchard, E. Payen, S. Inoue, H. Kudo, Y. Yoshimura, Appl. Catal. B 41 (2003) 181–191.
[6] M. Breysse, J.L. Portefaix, M. Vrinat, Catal. Today 10 (1991) 489–505.
[7] J. Ramirez, L. Cedeño, G. Busca, J. Catal. 184 (1999) 59–67.
[8] S. Inoue, A. Muto, H. Kudou, T. Ono, Appl. Catal. A 269 (2004) 7–12.
[9] H. Wang, Y. Wu, B.-Q. Xu, Appl. Catal. B 59 (2005) 139–146.
[10] O. Renn, M.C. Roco, J. Nanoparticle Res. 8 (2006) 153–191.
[11] R.W. Siegel, E. Hu, M.C. Roco (Eds.), Nanostructure Science and Technology, Springer (former Kluwer Academic Publishers), Dordrecht, Netherlands, 1999, available at http://www.wtec.org/loyola/nano/.
[12] C.N.H. Rao, M. Nath, Dalton Trans. 1 (2003) 1–24.
[13] V. Kozhukharov, P. Vitanov, E. Kabasanova, K. Kavasanov, M. Machkova, V. Blaskov, J. Environ. Prot. Ecol. 2 (2001) 107–111.
[14] N. Serpone, E. Pellizetti, Photocatalysis, Fundaments and applications, Wiley Interscience, New York, 1989, pp. 603–637.
[15] M. Schiavello, H. Dorrecht, Photochemistry, photocatalysis and photoreactors: fundamentals and developments, NATO Science Series C, Kluwer Academic, Boston, 1985.
[16] A.L. Linsebigler, G. Lu, J.T. Yates, Chem. Rev. 95 (1994) 735–758.
[17] R. Asahi, T. Morikawa, T. Ohwaki, K. Aoki, Y. Taga, Science 293 (2001) 269–271.
[18] M. Anpo, M. Takeuchi, Int. J. Photoenergy 3 (2001) 89–94.
[19] S.U.M. Khan, M. Al-Shahry, W.B.J. Ingler, Science 297 (2002) 2240–2243.
[20] T. Tachigawa, S. Tojo, K. Kawai, M. Endo, M. Fujitsuka, T. Ohno, K. Nishijima, Z. Miyamoto, T. Majima, J. Phys. Chem. B 108 (2004) 19299–19306.
[21] S. Sakthivel, H. Kisch, Angew. Chem. Int. 42 (2003) 4908–4911.
[22] T. Onho, T. Mitsui, M. Matsumura, Chem. Lett. 32 (2003) 364–365.
[23] S. Yin, K. Ihara, Y. Aita, M. Komatsu, T. Sato, J. Photochem. Photobiol. A: Chem. 179 (2006) 105–114.
[24] Y. Xie, X. Zhao, J. Mol. Catal. A: Chem. 285 (2008) 142–149.
[25] S. Sakthivel, H. Kisch, ChemPhysChem 4 (2003) 487–490.
[26] A. Ghicov, J.M.H. MacakTsuchiya, J. Kunze, V. Haeublein, L. Frey, P. Schmuki, Nano Lett. 6 (2006) 1080–1082.
[27] H. Kisch, S. Sakthivel, M. Janczarek, D. Mitoraj, J. Phys. Chem. C 111 (2007) 11445–11449.
[28] S. Livraghi, A. Votta, M.C. Paganini, E. Giamello, Chem. Commun. 4 (2005) 498–500.
[29] H. Yamashita, M. Harada, J. Misaka, M. Takeuchi, B. Neppolian, M. Anpo, Catal. Today 84 (2003) 191–196.
[30] K. Nagaveni, M.S. Hedge, G. Madras, J. Phys. Chem. B 108 (2004) 20204–20212.
[31] M. Alam-Khan, S. Ihl-Woo, O. Bong-Yang, Int. J. Hydrogen Energy 33 (2008) 5345–5351.
[32] W. Choi, A. Termin, M.R. Hoffmann, J. Phys. Chem. 98 (1994) 13669–13679.
[33] M.W. Xiao, L.S. Wang, X.J. Huang, Y.D. Wu, Z. Dang, J. Alloys Compd. 470 (2009) 486–491.
[34] F. Jiang, Z. Zheng, Z. Xu, S. Zheng, J. Hazard. Mater. 164 (2009) 1250–1256.
[35] F. Han, V.S.R. Kambala, M. Srinivasan, D. Rajarathnam, R. Naidu, Appl. Catal. A: Gen. 359 (2009) 25–40.
[36] A. Wood, M. Giersig, P. Mulvaney, J. Phys. Chem. B 105 (2001) 8810–8815.
[37] V. Subramanian, E.E. Wolf, P.V. Kamat, J. Phys. Chem. B 107 (2003) 7479–7485.
[38] M. Jakob, H. Levanon, P.V. Kamat, Nano Lett. 3 (2003) 353–358.
[39] V. Subramanian, E.E. Wolf, P.V. Kamat, J. Am. Chem. Soc. 126 (2004) 4943–4950.
[40] T. Hirakawa, P.V. Kamat, J. Am. Chem. Soc. 127 (2005) 3928–3934.

[41] P.D. Cozzoli, R. Comparelli, E. Fanizza, M.L. Curri, A. Agostiano, D. Baub, J. Am. Chem. Soc. 126 (2004) 3868–3879.
[42] T. Kasuga, M. Hiramatsu, A. Hoson, T. Sekino, K. Niihara, Langmuir 14 (1998) 3160–3163.
[43] G.H. Du, Q. Chen, R.C. Che, Z.Y. Yuan, L.M. Peng, Appl. Phys. Lett. 79 (2001) 3702–3704.
[44] J.A. Toledo-Antonio, S. Capula, M.A. Cortés-Jácome, C. Angeles-Chavez, E. López-Salinas, G. Ferrat, J. Navarrete, J. Escobar, J. Phys. Chem. C 111 (2007) 10799–10805.
[45] C. Cheng, H. Teng, Chem. Mater. 16 (2004) 4352–4358.
[46] T. Tachikawa, S. Tojo, M. Fujitsuka, T. Sekino, T. Majima, J. Phys. Chem. B 110 (2006) 14055–14059.
[47] L. Qian, Z.-S. Jin, S.-Y. Yang, Z.-L. Du, X.-R. Xu, Chem. Mater. 17 (2005) 5334–5338.
[48] H. Yu, J. Yu, B. Cheng, J. Lin, J. Harzard. Mater. 147 (2007) 581–587.
[49] H. Yu, J. Yu, B. Cheng, Chemosphere 66 (2007) 2050–2057.
[50] P. Gorska, A. Zaleska, E. Kowalska, T. Klimczuk, J.W. Sobczak, E. Skwarek, W. Janusz, J. Hupta, Appl. Catal. B 84 (2008) 440–447.
[51] H. Song, H. Jiang, H. Liu, X. Liu, G. Meng, Mater. Res. Bull. 42 (2007) 334–344.
[52] American Public Health Association (APHA), Standard Methods for the Examination of Water and Wastewater, 18th ed., American Public Health Association, USA, 1992.
[53] T. Gao, H. Fjellvåg, P. Norby, J. Phys. Chem. B 112 (2008) 9400–9405.
[54] R. Ma, K. Fukuda, T. Sasaki, M. Osada, Y. Bando, J. Phys. Chem. B 109 (2005) 6210–6214.
[55] E. Morgado Jr., M.A.S. de Abreu, G.T. Moure, B.A. Marinkovic, P.M. Jardim, A.S. Araujo, Mater. Res. Bull. 42 (2007) 1748–1760.
[56] Z.Y. Yuan, J.F. Colomer, B.L. Su, Chem. Phys. Lett. 363 (2002) 262–366.